PHYSICAL REVIEW B VOLUME 15, NUMBER 2 15 JANUARY 1977

X-ray scattering from adsorbed xenon monolayer films

George W. Brady* and David B. Fein
Bell Laboratories, Murray Hill, New Jersey 07974

William A. Steele
Department of Chemistry, Pennsylvania State University, University Park, Pennsylvania 16802
(Received 7 April 1976)

The x-ray diffraction patterns of xenon adsorbed on spheron have been measured at 175°K for surface coverages from $\theta = 0.1$ to 1.05. Continuous patterns of a liquidlike character are obtained, without any obvious change in the structure of the adsorbed film with coverage. Atomic distribution functions were calculated by Fourier transforming the xenon structure factor. Theoretical arguments are advanced concerning these distribution functions and structure factors. It is concluded that the adsorbed films show no sign of registry with the surface lattice or long-range two-dimensional order under the experimental conditions of this study.

I. INTRODUCTION

The properties of simple gases physically adsorbed on well-characterized solid surfaces have recently become a subject of renewed interest.[1,2] Heat-capacity and isotherm measurements on rare gases adsorbed on graphitized carbon blacks indicate an unexpected variety of phase transitions in these two-dimensional systems,[2-7] including ordered films which may or may not be in registry with the substrate lattice; as well as liquidlike films which exhibit two-phase equilibriums and two-dimensional critical points. Although some of these phenomena were well known, recent data have allowed a better definition of the two-dimensional phase diagrams as well as revealing entirely new phases in some systems. In addition to the thermodynamic investigations, structural studies that yield information concerning the atomic distributions in these films are of considerable interest. These include low-energy electron diffraction (LEED) measurements on physisorbed films at very low temperatures[8] (where the vapor pressure of the adsorbed gas is small so that scattering from unadsorbed gas does not obscure the diffraction pattern) and more recently, determinations of neutron diffraction by physisorbed films.[9] In the neutron-diffraction study, the substrate consisted of exfoliated graphite oriented so that the basal planes were nearly parallel to one another and to the wave vectors of the incident and scattered neutron beam. Films of ^{36}Ar and N_2 were adsorbed (primarily on the basal planes) at coverages near to or greater than one monolayer. Under these conditions, measurable changes in the neutron scattering occurred when gas was adsorbed; observed features in the difference spectra were related to the adatom-adatom ordering that occurs in these systems at the relatively low temperatures used.

In this paper, we report x-ray scattering from xenon physisorbed on a graphitized carbon black. These experiments have several advantageous features relative to the electron- and neutron-diffraction techniques. Quantitative data can be obtained even when the equilibrium gas pressure is large or when the surface coverage is low. A powdered solid can be used, thus greatly enlarging the future choice of possible adsorbents (relative to the small number that occurs with macroscopically parallel substrate planes). In addition, use of a powdered sample means that the scattered intensity is due to the adatom-substrate spatial distribution as well as the adatom-adatom distribution. Indeed, we will see that the diffraction features are predominantly due to the adatom-substrate distributions. This is of particular interest in connection with determination of the degree of registry between the adatoms and the surface lattice, since registry clearly means that a particular set of adatom-solid atom distances are favored. Although determinations of the adatom-adatom lattice size and symmetry are indicative of the formation of a registered layer, a final answer to this question can only be given if one knows whether the two two-dimensional lattices (adatom and solid surface) are ordered relative to one another.

As a first system for study we chose xenon on graphitized spheron (a carbon black), primarily because of the favorable ratio of scattering factors of the two components; these are very roughly proportional to their atomic numbers, that is, 54 to 6. Since at one monolayer there are $\sim 10^{-2}$ atoms adsorbed per atom of this substrate, scattering at less than monolayer coverage should be detectable. In a two-component system of this kind the scattering is given by[10]

$$I = I_{\mathrm{XeXe}} + I_{\mathrm{XeC}} + I_{\mathrm{CC}} , \tag{1.1}$$

where the subscripts are self-explanatory. The substrate scattering I_{CC} can be directly subtracted from the raw data after suitable absorption corrections[11] have been applied. The scattering of the surface system is then given by the remaining two terms, which can be written

$$\Delta I(s) = \left\langle f_{Xe}^2 \sum_{\substack{Xe \\ atoms}} e^{i\vec{s}\cdot\vec{r}_{Xe\text{-}Xe}} + 2 f_{Xe} f_C \sum_{\substack{C \\ atoms}} e^{i\vec{s}\cdot\vec{r}_{Xe\text{-}C}} \right\rangle , \tag{1.2}$$

where $\Delta I(s)$ is the excess scattering per xenon atom and $\vec{s}$ is the usual scattering vector with length equal to $(4\lambda/\lambda)\sin\theta$, where λ is the x-ray wavelength and θ is $\frac{1}{2}$ the scattering angle. The angular brackets in Eq. (1.2) indicate an average over all crystallite orientations in the powdered sample, and the sums are to be taken over all Xe atoms in the film and C atoms in the solid adsorbent, respectively. We define a coordinate system with z perpendicular to and $\vec{\tau}$ a vector parallel to the surface. If the orientation of $\vec{s}$ in these coordinates is denoted by Ω_S and the orientation of $\vec{r}_{Xe\text{-}Xe}$ by Ω_{Xe}, we have

$$e^{i\vec{s}\cdot\vec{r}_{Xe\text{-}Xe}} = 4\pi \sum_l i^l j_l(s r_{Xe\text{-}Xe}) Y_{lm}(\Omega_S) Y_{lm}^*(\Omega_{Xe}) . \tag{1.3}$$

An average of the spherical harmonic $Y_{lm}(\Omega_S)$ over a random distribution of crystallite orientations immediately gives

$$\langle e^{i\vec{s}\cdot\vec{r}_{Xe\text{-}Xe}} \rangle = \frac{\sin s r_{Xe\text{-}Xe}}{s r_{Xe\text{-}Xe}} . \tag{1.4}$$

A similar result is obtained for the Xe-C vectors. Thus,

$$\Delta I(s) = f_{Xe}^2 \left(1 + \sum_{Xe\ atoms}{}^{*} \frac{\sin s r_{Xe\text{-}Xe}}{s r_{Xe\text{-}Xe}} + 2 \frac{f_C}{f_{Xe}} \sum_{C\ atoms} \frac{\sin s r_{Xe\text{-}C}}{s r_{Xe\text{-}C}} \right) , \tag{1.5}$$

where the asterisk on the summation means that the "self" term ($r_{Xe\text{-}Xe} = 0$) has been split off. This expression shows quite clearly that the Fourier transform of $\Delta I(s)/f_{Xe}^2$ yields a linear combination of the distribution of Xe–C and Xe–Xe distances. A distribution function $\rho(r)$ is defined by

$$\rho(r) = \frac{1}{2\pi^2} \int_0^\infty \frac{\sin s r}{s r} \left(\frac{\Delta I(s)}{f_{Xe}^2} - 1 \right) s^2 \, ds . \tag{1.6}$$

Even though $\rho(r)$ could be calculated with reasonable precision from the data, its relationship to the Xe-Xe distribution or the Xe-C distribution is far from trivial; for this reason, a careful theoretical analysis is presented in Sec. III which will serve as a guide in interpreting the experimental $\rho(r)$ as well as relating the diffracted intensities to the atomic distributions.

II. EXPERIMENTAL

The adsorbent used in this work was a sample of spheron 6 which had been heated for 2 h at 2700 °C in a reducing atmosphere. The resulting graphitized carbon black is commonly known as graphon, and was kindly provided to one of us (W.A.S.) by Dr. Walter Smith of the Godfrey Cabot Corporation. The surface area of this solid is ~80 m^2/g [by the BET (Brunauer-Emmett-Teller) method, using N_2 gas]; more importantly, the quantity of xenon required to form a complete monolayer (at 90 °K) is precisely known to be 7.8×10^{-4} moles/g solid. The fractional coverage θ shown in Fig. 2 is calculated by combining the measured equilibrium pressures with the published isotherms of Cochrane *et al.*[12] for the same system. The coverages were also calculated from the sample x-ray absorption. To do this the transmission was determined by measuring the area of the $(10\bar{1})$ reflection of the Be cell windows, before and after the Xe was adsorbed. The x-ray absorption of the gas above the sample was corrected for when necessary by measuring the transmission for various pressures of Xe at room temperature, where the surface adsorption was negligible. A simple temperature proportionality was then used to convert the densities at room temperature to those corresponding to the sample temperature. Repeating the same measurements at the experimental temperature then gave the x-ray attenuation due to the absorbed film plus the graphon substrate. From this the fraction θ of surface covered could be calculated. Thus,

$$I_C/I_0 = e^{-\mu_C m_C} , \tag{2.1}$$

where I_0 and I_C are the peak intensities of the $(10\bar{1})$ Be peaks with the cell empty and filled with graphon, respectively; and μ_C, m_C are the mass absorption coefficient and the mass of the graphon, respectively. Denoting these quantities for Xe by μ_{Xe} and m_{Xe}, and setting I_{Xe} equal to the intensity of the sample with absorbed Xe, we have

$$\frac{I_{Xe}}{I_C} = \frac{e^{-(\mu_C m_C + \mu_{Xe} m_{Xe})}}{I_0 e^{-\mu_C m_C}} = \frac{e^{-\mu_{Xe} m_{Xe}}}{I_0} . \tag{2.2}$$

The absorption coefficients are $\mu_C = 5.50\ g^{-1}$ and $\mu_{Xe} = 330\ g^{-1}$. From Eqs. (2.1) and (2.2), the values of m_C and m_{Xe} in grams can be calculated. Dividing m_{Xe} by m_C then gives the number of grams of Xe absorbed per gram of graphon. Coverages cal-

culated by the two methods agreed within 2%.

The x-ray scattering apparatus consisted of a metal vacuum system evacuated by a Vac-ion pump. With the exception of the thermostat all the components were obtained from Varian Vacuum Products. A diagram is shown in Fig. 1. The thermostat, the inner jacket of which was a copper container for liquid N_2, was mounted at the top of a vertical column constructed from $2\frac{3}{4}$ in. stainless-steel tubing. At the lower end of the column a stainless-steel cross fitting with flanges allowed attachment to the pumps and an ion gauge. Further up the column, a horizontal take-off arm 75 cm in length was attached through a cross fitting and the x-ray chamber was mounted at the end of it. Soldered to the bottom of the copper container was a $\frac{3}{8}$-in. copper rod that ran down the axis of the vacuum column, then at right angles out to the scattering chamber. It served as the heat sink and conductor between the liquid N_2 reservoir and the sample cell. This latter was made by cutting a section 1.3-cm long by 0.5-cm wide out of the rod. A ridge 0.12-cm thick was left in the center of the rod, to which Be windows could be cemented. The ridge and thus the cell windows, were tilted at an angle of 45° to the vertical to allow measurements of the scattering between Bragg angles of 0° and 90°. Gas inlet holes were drilled through the rod and ridge at right angles to the plane of the cell windows. The cell was filled with graphon by first cementing the lower Be window to the ridge with Torrseal, packing in the graphon firmly, and then attaching the other Be window, also with Torrseal.

The gas adsorption chamber surrounding the end of the rod holding the graphon-Be window arrangement was made of $\frac{3}{4}$-in. tubing. It was sealed off from the main vacuum system by a glass-to-metal seal between the metal rod and the inner wall of the tubing, but was connected to the gas handling system through a vacuum valve. X-ray ports were machined out of the tubing: the entrance port was 3-mm wide and 1.3-cm long. The exit port, of the same length, was wide enough to allow passage of the radiation scattered between angles of $-1°$ and 90°. Mylar windows 0.004-in. thick were placed over the ports, and sealed to the metal jacket with Torrseal. Sample temperatures were measured with a copper-constantan thermocouple placed in a well in the inner copper rod adjacent to the sample.

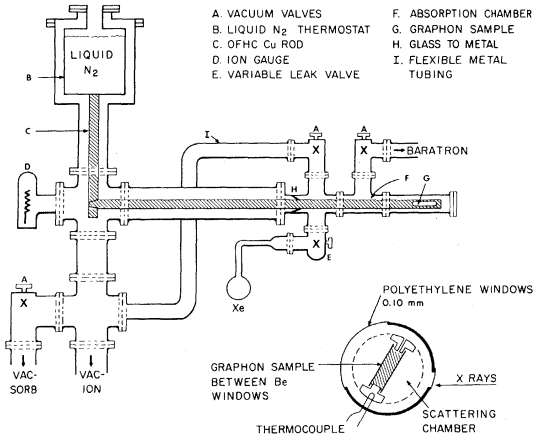

FIG. 1. Schematic diagram of the apparatus. Scattering chamber is shown in the inset; the chamber is shown together with the system for its temperature control in the main part of the figure.

The system was outgassed by pumping at a temperature of 125 °C for two weeks. After this period, the pressure as read on the ion gauge was below 10^{-8} Torr.

Research grade (99.99%) Xe gas was admitted into the adsorption chamber through a variable leak valve. Pressures were read on a Baratron gauge.

The temperature was controlled by first filling the thermostat with liquid N_2. After equilibration, the temperature at the sample was 148 °K. This temperature was adjusted upward by admitting air to that portion of the vacuum system enclosed by the vertical column and the side arm out to the scattering chamber. The thermal conductivity increases between the inner copper rod and the external walls then caused the temperature to rise. The extent of the rise could be easily controlled by adjusting the air pressure. Since each coverage of absorbed xenon corresponded to a different pressure in the sample container and thus to a different thermal conductivity at that point, different air pressures were needed to maintain a constant temperature at the sample. Icing of the cell windows was prevented by a stream of nitrogen flowing over the cell windows. The final sample temperature used was 178 °K, and was stable to within 0.1 °C over the period of the experiment.

The radiation used was Cu$K\alpha$, monochromated by reflection from a singly bent LiF crystal. Absorption corrections were measured, and applied to all the curves by methods previously described.[11] When done in this way, the corrected scattering curves for graphon could be subtracted directly from the curves for the different surface coverages to give the scattering due to the adsorbed Xe films. Polarization corrections were applied, and the incoherent part of the scattering removed by the method of Warren.[13] The curves shown in Fig. 2 thus represent the corrected coherent scattering of the adsorbed films.

Figure 2 shows that even at fractional coverages

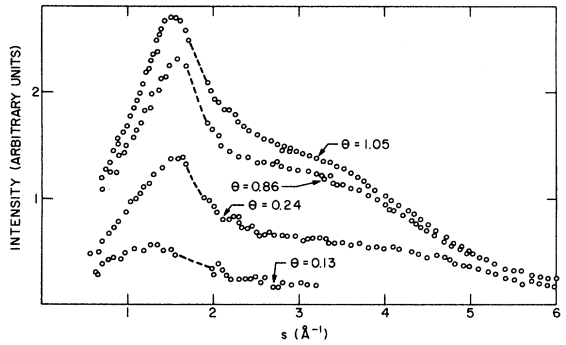

FIG. 2. Total excess scattering curves for different coverages of xenon on graphon. Fraction of surface covered, θ, for each curve is shown. Dashed portions between $s = 1.5$ and 2.0 Å^{-1} show the position and width of the (002) carbon peak.

as low as $\theta = 0.13$, significant scattering is observed although at this low coverage the scattering is detectable only out to $s \simeq 3$, and the only detail visible is a broad maximum centered at $s \simeq 1.5$; the peak position is uncertain because of the low scattering relative to the tail of the (002) graphite line (the region of overlap is shown as a dashed portion of each of the curves). At the higher coverages complete patterns were obtained, although the data could be recorded only out to $s = 6.0$ Å^{-1} because of the experimental arrrangements for this work. The features of the patterns are not those of a system whose structure is changing in any marked way with coverage. In fact, outside of a fairly continuous sharpening and shift towards lower angle of the broad peak centered at $s \sim 4.0$ Å^{-1} in curve 2, and the gradual disappearance of a slight shoulder on the left of the first peak at $s \sim 1.4$ Å^{-1} the curves are strikingly similar considering that the mole fraction of one of the components, the adsorbed xenon, has changed by a factor of 10. The structure factors $H(s) = \Delta I / f_{Xe}^2 - 1$ are shown in Fig. 3. Considerable care was required in evaluating $H(s)$ because of the difficulty in deciding the magnitude of f_{Xe}^2 (in arbitrary units). Since the experimental range of s was so limited, it seemed quite possible that scattering from Xe-C and Xe-Xe correlations would be non-negligible even at the largest s values. The criterion adopted was to set $\Delta I = f_{Xe}^2$ at a value of s such that the negative values of the structure factor in the region of $s = 4.5$ to 6.0 Å passed through a minimum and began to increase towards zero. The region where the curve fitting has to be done is also the region where the absorption correction is greatest, and where ΔI is minimal, but the net effect of an error in this procedure would be to displace the curves of $H(s)$ up or down, and to change the ratios of the peak intensities. The main thrust of our analysis will be a comparison of calculated and measured structure factors, and we will take account of these uncertainties in $H(s)$ in the discussion.

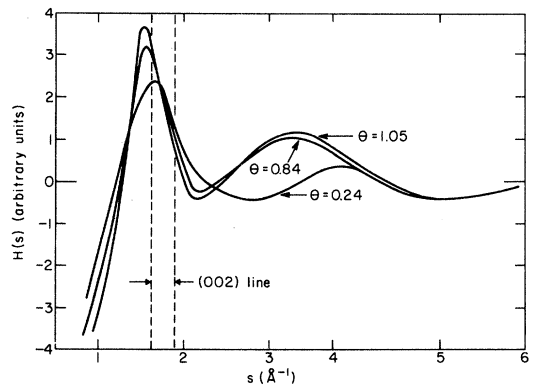

FIG. 3. Experimental structure factors for three of coverages of Fig. 2. (002) carbon peak lies between the dashed lines.

Fourier transforms of the data are shown in Fig. 4. Because of the small range of s measured, direct transformation gave curves whose features were badly masked by termination error. To overcome these difficulties the curve of $\Delta I / f_{Xe}^2 - 1$ was extended by drawing a straight line from the observed value at $s = 6.0$ Å^{-1} to zero at $s = 16$ Å^{-1}.[14] The upper limit of $s = 16$ Å^{-1} is a physically realizable limit and was chosen to minimize termination error.[13] The straight-line extrapolation was selected over other functional forms (such as a Gaussian) because it could be conveniently inserted into our computer pro-

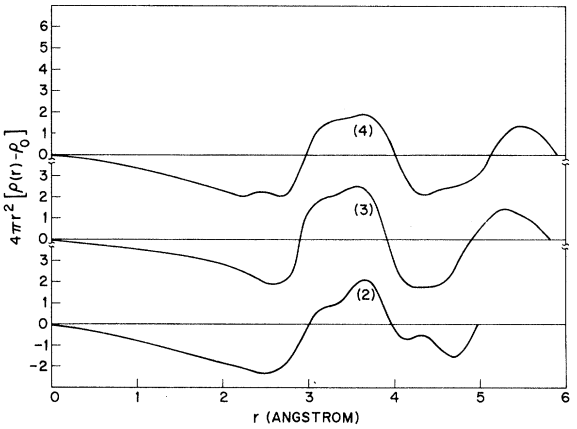

FIG. 4. Fourier transforms of the xenon structure factors of Fig. 3. Because of the small range of s covered there is still some ripple in the curves; the relative values of the ordinate from curve to curve are not too significant because of uncertainty in the curve fitting.

gram. The Fourier transform of the extrapolated part of the curve is a ripple curve of constant periodicity and low amplitude which does not interfere with the interpretation of the data. The Fourier transform was then reiterated by setting all values of $r\rho(r)$ to the left of the peak at $r \simeq 3$ Å to 0, transforming back to s space and then transforming again to obtain a corrected $r\rho(r)$.[15] In this way the error resulting from the approximate first fit of I to f^2_{Xe} in the curve-fitting procedure is minimized. What results from these operations is a set of distribution functions which are markedly similar at all three coverages, although there are slight shifts from curve to curve. There is evidence of residual ripple in all the curves, but since no quantitative significance can be attached to the curves (because of the limited range of s), we will only use the curves of Fig. 4 in a qualitative way to indicate that there are peaks in the region between 3 and 4 Å in all the curves and another broad peak at ~5.5 Å. At the lowest coverage the peak at 3.7 Å is well defined, and if we assume that the feature at ~3.2 is a ripple effect, the 3.7 Å distance would appear to be quite definite at this coverage. At the two higher coverages the maximum is shifted slightly to the right. These peaks are to be attributed to nearest-neighbor correlations. The peak at 5.5 Å suggests that there is scattering matter at a distance intermediate between that expected for first and second neighbors. It is not fruitful to draw further conclusions from the distribution functions until a more complete set of data is measured. We point out, however, that these curves, obtained for the first time for monolayers, show the inherent power of the diffraction method in elucidating the structure of the adsorbed films. We will return to a discussion of the experimental curves in a later section.

III. THEORY

One of the advantages of choosing xenon on graphon for study is that this happens to be a relatively well-characterized absorbate-absorbent system. Extensive thermodynamic measurements have been reported for the rare gases adsorbed on this solid and on similar graphitized carbon blacks[16] which allow one to state with some confidence that the surface is uniform, containing ~0.5% heterogeneous area. An extrapolation of the experimental heats of adsorption to zero coverage allows one to estimate the average energy of an isolated adsorbed Xe atom on the uniform part of the surface (relative to an atom in free space with zero kinetic energy). Furthermore, x-ray and electron diffraction studies of this adsorbent have been reported which indicate that it is made up of crystallites with mostly basal planes exposed, with an average thickness of 40 Å and an average area of ~4200 Å^2.[17] Since the interplanar separation is 3.45 Å and the unit lattice-cell dimension in the basal plane is 2.46 Å, each crystallite can be thought of as a stack of 12 basal planes, with each plane containing ~700 unit cells. Furthermore, the shapes of the x-ray peaks indicate that neighboring basal planes are essentially randomly distributed with respect to rotations and translations in the planes.[18] For convenience, we will take the planes to be circular, with radius 37Å. LEED studies[8] on the Xe-graphitized carbon black system indicate that adsorbed xenon in a dense monolayer can be in registry with the graphite lattice, with $\frac{1}{3}$ of the adsorption sites occupied. This corresponds to a Xe-Xe separation of $\sqrt{3}\,d_{s\text{-}s}$ where $d_{s\text{-}s}$ is the site-site separation of 2.46 Å. The distance of 4.26 Å obtained in this way happens to be quite close to the Xe-Xe separation in the bulk crystal at 0 °K (4.31 Å) and to the distance corresponding to the minimum interaction energy of a pair of Xe atoms (4.46 Å). Since the close-packed two-dimensional lattice has the same triangular symmetry as a $\sqrt{3} \times \sqrt{3}$ lattice in registry with the carbon basal plane and the expected dimensions are quite similar in both cases, it is possible that the role of the substrate in this case is to encourage and perhaps to slightly compress an ordered two-dimensional array that forms due to the Xe-Xe interactions. In any case, experiments such as those reported in this paper should help to determine the range of coverage and temperature where an ordered array exists. Even when one works outside the ordered region of the phase diagram, diffraction measurements can yield information concerning a more subtle aspect of the structure of adsorbed films: namely, whether partial registry persists in monolayers that lack long-range order. (This point bears on the question of the reality of sitewise adsorption models for disordered films.) However, interpretation of our data requires a theoretical description of the diffraction from partially ordered films. A suitable theory is presented here.

In addition to previous experimental investigations of the Xe-graphitized carbon black system theoretical studies of the interaction of an isolated Xe atom with the surface have been presented which seem to be reasonably realistic.[19] Since these calculations provide helpful background information for interpreting the x-ray data, we briefly summarize them. It is generally assumed that the interaction energy $u_s(\vec{r})$ can be represented

as a sum of pairwise Xe-C atom interactions:

$$u_s(\vec{r}) = 4\epsilon_{\text{Xe-C}} \sum_{\text{lattice}} \left[\left(\frac{\sigma_{\text{Xe-C}}}{r_i} \right)^{12} - \left(\frac{\sigma_{\text{Xe-C}}}{r_i} \right)^{6} \right]. \tag{3.1}$$

The constant $\epsilon_{\text{Xe-C}}$ is estimated by taking the geometric mean of the well depths $\epsilon_{\text{Xe-Xe}}$ and $\epsilon_{\text{C-C}}$ for like-atom interactions and will here be taken to be 80 °K: the size parameter $\sigma_{\text{Xe-C}}$ is assumed to be the arithmetic mean of $\sigma_{\text{Xe-Xe}} = 3.98$ Å and the interplanar spacing in graphite of 3.40 Å.

The summation over the lattice in Eq. (3.1) can be carried out directly on a computer: however, for many purposes, it is most convenient to use the symmetry of $u_s(\vec{r})$ to express it as a Fourier series. If we assume that the basal planes are perfect and infinite in size, $u_s(\vec{r})$ has a periodicity in two dimensions which is identical to the periodicity of the basal plane. Thus, if $\vec{\tau}$ is the two-dimensional vector parallel to the surface and z is perpendicular to it, one can write

$$u_s(\vec{r}) = \sum_{\vec{g}} w_{\vec{g}}(z)\, e^{i\vec{g}\cdot\vec{\tau}}, \tag{3.2}$$

where $\vec{g}$ is a multiple of the reciprocal-lattice vectors $\vec{b}_1$, $\vec{b}_2$:

$$\vec{g} = 2\pi(g_1\vec{b}_1 + g_2\vec{b}_2). \tag{3.3}$$

Explicit expressions for the coefficients $w_{\vec{g}}(z)$ are given elsewhere. For present purposes, it is important to note that the periodicity of $u_s(\vec{r})$ is sufficiently weak to allow one to truncate the series in Eq. (3.2) after the first set of g vectors of length $4\pi/\sqrt{3a} = 2.95$ Å^{-1}. Thus, one can write

$$u_s(\vec{r}) = w_0(z) + w_1(z)[\cos 2\pi S_1 + \cos 2\pi S_2 + \cos 2\pi(S_1 + S_2)], \tag{3.4}$$

where the position vector has been written as a multiple of the lattice vectors: thus $\vec{\tau} = S_1\vec{a}_1$, $S_2\vec{a}_2$.

Explicit calculations of $u_s(\vec{r})$ suggest that the average separation distance between an adsorbed xenon atom and the graphite basal plane should be between 3.6 and 3.7 Å; furthermore, at 180 °K, a harmonic oscillator approximation indicates that this atom will have a mean-square displacement perpendicular to the surface $\langle(\delta z)^2\rangle$ amounting to ~0.06 Å^2. [We note that the calculated average energy of an isolated adsorbed xenon atom is $-1830 + \frac{3}{2}T = -1560$ °K at 180°, which agrees well with the value of −1580 °K obtained from the experimental heats of adsorption.[16] Coulomb *et al.*[8] have measured the mean-square displacement of xenon atoms on graphite; their results give ~0.05 Å^2 (for an isolated xenon atom) at 180 °K.] The barriers to free translation of a xenon atom on the surface amount to 40 °K and thus are small compared to T at the experimental temperature; in other words, the periodic component of $u_s(\vec{r})$ which might cause the adsorbed xenon to be in registry with the substrate is quite small. (We emphasize that the coverage and temperature ranges of this x-ray study do not overlap those of the LEED investigation.) It is interesting to note that the radial distribution functions shown in Fig. 4 exhibit a broad maximum in the region between 3.6 and 3.7 Å. However, in order to associate this with the Xe-graphite lattice separation distance, it is necessary to carry out a more detailed analysis of the experimental scattering and the distribution function which results when the sine transform is evaluated.

In order to evaluate the sums in Eq. (1.5) or to understand the distribution functions shown in Fig. 4, we find it convenient to introduce the probability densities for Xe-C and Xe-Xe distances. Thus, we define $\rho_C G_{\text{Xe-C}}(\vec{r})$ to be the number of carbon atoms in unit volume located at point $\vec{r}$ relative to a xenon atom (we continue to use the surface-oriented coordinate axes defined in Sec. I). If ρ_C is the number of carbon atoms per unit volume, $G_{\text{Xe-C}}(\vec{r})$ is a pair correlation as usually defined,

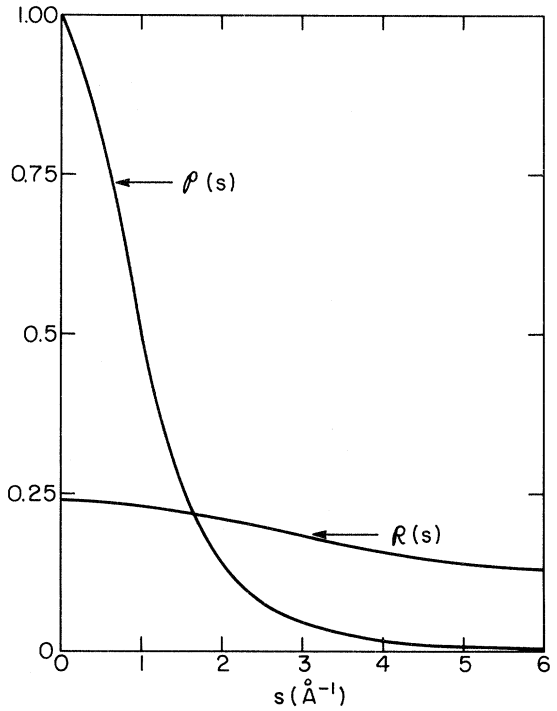

FIG. 5. Behavior of the relevant atomic scattering factors is shown here. Square of the normalized scattering factor for xenon and the ratio of the carbon to the xenon factor are denoted by $\mathcal{P}(s)$ and $\mathcal{R}(s)$, respectively.

except that it is a vector function. As we will see later, $G_{\text{Xe-C}}(\vec{r})$ can be discontinuous and approaches a sum of δ functions in the limit of complete ordering. Equation (1.5) can now be written

$$H(s) = \frac{\Delta I(s)}{f_{\text{Xe}}^2} - 1 = \frac{2f_C\rho_C}{f_{\text{Xe}}} \int_V G_{\text{Xe-C}}(\vec{r}) \frac{\sin sr}{sr}\, d\vec{r} + \int_V \rho_{\text{Xe-Xe}}(\vec{r}) \frac{\sin sr}{sr}\, d\vec{r}, \quad (3.5)$$

where $H(s)$ is the experimental structure factor. The atomic scattering factor for xenon and carbon can be obtained from the International Tables[20]; we define:

$$\mathcal{R}(s) = f_C(s)/f_{\text{Xe}}(s). \quad (3.6)$$

Figure 5 shows a curve of $\mathcal{R}(s)$ calculated from the Tables; it is interesting to note that $\mathcal{R}(s)$ is a slowly-varying function of s. Indeed little error would be introduced if one merely sets $\mathcal{R}(s) \simeq 0.22$ in the subsequent development. In any case, we now have

$$H(s) = 2\rho_C\left(\mathcal{R}(s)\int_{V_C} G_{\text{Xe-C}}(\vec{r}) \frac{\sin sr}{sr}\, dr + \frac{1}{2}\int_{V_C} \frac{\rho_{\text{Xe-Xe}}(\vec{r})}{\rho_C} \frac{\sin sr}{sr}\, d\vec{r}\right), \quad (3.7)$$

$$H(s) = 2\rho_C[\mathcal{R}(s)H_{\text{Xe-C}}(s) + \tfrac{1}{2}H_{\text{Xe-Xe}}(s)], \quad (3.8)$$

where V_C is the volume of a solid crystallite.

We begin by focusing on the structure factor arising from Xe-C diffraction and write the first integral in Eq. (3.8) as

$$H_{\text{Xe-C}}(s) = \left(\frac{\pi}{2}\right)^{1/2} \int_z \int_a G_{\text{Xe-C}}(\vec{r}) \frac{J_{1/2}(sr)}{(sr)^{1/2}}\, dz\, d\vec{\tau}, \quad (3.9)$$

where $\mathcal{A}$ is the basal plane area of an adsorbent crystallite, Z is its thickness, and the Bessel function $J_{1/2}(x) = (\frac{1}{2}\pi x)^{-1/2}\sin x$. Consider now $G_{\text{Xe-C}}(\vec{r})$, the correlation between a xenon atom and the graphite lattice; if we assume that the xenon atom is adsorbed on a perfect basal plane of infinite size, we see that $G_{\text{Xe-C}}(\vec{r})$ has translation symmetry of the basal plane; that is, a translation of the xenon from a position above one unit lattice cell to an identical position above a different lattice cell leaves $G_{\text{Xe-C}}(\vec{r})$ unchanged. Formally, this means that

$$G_{\text{Xe-C}}(z, \vec{\tau}) = G_{\text{Xe-C}}(z, \vec{\tau} + m_1\vec{a}_1 + m_2\vec{a}_2), \quad (3.10)$$

where m_1 and m_2 are integers. An important consequence of this symmetry property is that $G_{\text{Xe-C}}(\vec{r})$ can be written in terms of a Fourier expansion

$$G_{\text{Xe-C}}(r) = \sum_{\vec{g}} G_{\vec{g}}(z)\, e^{i\vec{g}\cdot\vec{\tau}}, \quad (3.11)$$

where the $\vec{g}$ vectors have been defined in Eq. (3.3). When Eq. (3.10) is substituted into Eq. (3.9) together with $r = (z^2 + \tau^2)^{1/2}$, one can write

$$H_{\text{Xe-C}}(s) = 2\pi\left(\frac{\pi}{2}\right)^{1/2} \sum_{\vec{g}} \int_Z G_g(z)\, dz \times \int_0^\infty \frac{J_{1/2}[s(\tau^2+z^2)^{1/2}]}{[s(\tau^2+z^2)^{1/2}]^{1/2}} \times J_0(g\tau)\tau\, d\tau. \quad (3.12)$$

The integral is given by Watson[21] [Sec. (13.47)]; the result can be written

$$H_{\text{Xe-C}}(s) = \sum_{\vec{g}} f_{\vec{g}}(s). \quad (3.13)$$

For finite g,

$$f_{\vec{g}}(s) = \begin{cases} 0, & s < g \\ \dfrac{2\pi}{s(s^2-g^2)^{1/2}} \displaystyle\int_z G_{\vec{g}}(z)\cos[z(s^2-g^2)^{1/2}]\, dz, & s > g. \end{cases} \quad (3.14)$$

However, when $g = 0$, it is necessary to integrate only up to R, the radius of the basal plane of the crystallite, and one finds

$$f_0(s) = \frac{2\pi}{s^2}\int_Z G_0(z)\{\cos(sz) - \cos[s(R^2+z^2)^{1/2}]\}dz. \quad (3.15)$$

Of course, the integrations for $f_g(s)$ when $g \neq 0$ should also be truncated at R rather than infinity; we return to this point after considering the z dependence of the xenon-graphite correlation functions.

The calculated potential energy curves serve to reinforce the belief that xenon physisorbed on a graphite basal plane is solidlike in at least one respect: namely, that the distances of a xenon atom from the surface are well defined, being equal to z_{eq} (plus or minus a small vibrational displacement). Furthermore, the variations in z_{eq} with τ are likely to be small enough to be negligible. Consequently, we can write a first approximation to the z dependence of $\rho_{\text{Xe-C}}(\vec{r})$ which is

$$\rho_{\text{Xe-C}}(\vec{r}) = \sum_{n=0}^{N_z-1} \rho_{\text{Xe-C}}(z_n)\,\rho_{\text{Xe-C}}(\vec{\tau}_n), \quad (3.16)$$

$$\rho_{\text{Xe-C}}(z_n) = \delta(z - (z_{\text{eq}} + nd)), \quad (3.17)$$

where N_z is the total number of basal planes in a crystallite and d is the distance between adjacent

basal planes. The sum in Eq. (3.16) reflects the fact that we need the probability of finding *any* plane of carbon atoms, surface or not, at a distance z from the xenon atom. We recollect that

$$G_{\vec{g}}(z)=\frac{1}{\mathcal{A}}\int_{\mathcal{A}}\frac{\rho_{\text{Xe-C}}(\vec{r})}{\rho_C}e^{-i\vec{g}\cdot\vec{\tau}}d\vec{\tau}. \tag{3.18}$$

When Eqs. (3.16) and (3.17) are substituted into Eq. (3.18), the result can be written

$$G_{\vec{g}}(z)=d\sum_{n=0}^{N_z-1}a_{\vec{g}}(n)\,\delta(z-(z_{\text{eq}}+nd)), \tag{3.19}$$

where the $a_{\vec{g}}(n)$ are dimensionless coefficients that characterize the magnitude of the correlation between the periodic variations in xenon density in the plane parallel to the surface and the positions of the carbon atoms in the nth plane. The normalization of $G_{\text{Xe-C}}(\vec{r})$ requires that

$$\int_{V_C}G_{\text{Xe-C}}(\vec{r})\,d\vec{r}=V_C\equiv d\mathcal{A}\,N_z. \tag{3.20}$$

Thus, we find that

$$a_0(n)\equiv 1. \tag{3.21}$$

In order to clarify the meaning of the $a_{\vec{g}}(n)$, we pause a moment to specify these coefficients for two limiting cases of interest.

(a) A completely mobile film in which there is no periodic variation in $\rho_{\text{Xe-C}}(\vec{r})$; for this case,

$$a_{\vec{g}}(n)=0 \quad \text{for } \vec{g}\neq 0. \tag{3.22}$$

(b) A completely registered overlattice in which the xenon atoms are located at the adsorption sites. In this case

$$\rho_{\text{Xe-C}}(\vec{\tau}_0)=\sum\delta(\vec{\tau}-\vec{\tau}_C), \tag{3.23}$$

where $\vec{\tau}_C$ denotes the location of a carbon atom in the surface basal plane relative to an origin that coincides with an adsorption site. If these sites are at the centers of the carbon hexagons,

$$\vec{\tau}_C=(m_1\pm\tfrac{1}{3})\vec{a}_1+(m_2\pm\tfrac{1}{3})\vec{a}_2, \tag{3.24}$$

where m_1 and m_2 are integers. When Eqs. (3.16), (3.23), and (3.24) are substituted into Eq. (3.18), the result can be compared with Eqs. (3.17) and (3.19) to show

$$a_{\vec{g}}(0)=\begin{cases}-\frac{1}{2}, & g_1+g_2\neq 3k\\ 1, & g_1+g_2=3k,\end{cases} \tag{3.25}$$

where k is an integer. Note that this result is obtained regardless of the spacing in the registered lattice (i.e., there is no difference between the 1×1 and $\sqrt{3}\times\sqrt{3}$ overlayer, for example). It is only when one considers the contribution to the diffracted intensity due to adatom-adatom correlations that the spacing in registered overlayers begins to play an important role.

A more refined expression for the z dependence of the Xe-C density than that given in Eq. (3.17) would allow for thermal vibration of the xenon atoms. Thus, one might write

$$\rho_{\text{Xe-C}}(z_n)=\left(\frac{1}{2\pi D^2}\right)^{1/2}\exp\left(-\frac{(\delta z_n)^2}{2D^2}\right), \tag{3.26}$$

where D is the root-mean-square amplitude of vibration in the z direction and

$$\delta z_n=z-(z_{\text{eq}}+nd). \tag{3.27}$$

The consequence of using Eq. (3.26) rather than Eq. (3.17) is to introduce a Debye-Waller factor in the expressions for the $f_g(s)$.

In either case, we see that evaluation of the $f_{\vec{g}}(s)$ requires a summation over carbon planes. In order to perform this summation over n, one can go more deeply into the characterization of $a_{\vec{g}}(n)$ for gases adsorbed on this solid. We recollect that these coefficients are a measure of the correlation between xenon and carbon atom positions. If we make the trivial assumption that $\vec{\tau}$ dependence of these correlations is due to interactions with the surface basal plane, the experimental observation[18] of a random distribution of nonsurface basal planes with respect to a $\vec{\tau}$ vector defined relative to the surface lattice immediately leads to the conclusion that

$$a_{\vec{g}}(n)\equiv 0 \quad \text{for } n>0,\ g>0, \tag{3.28}$$

regardless of the degree of registry between the xenon layer and surface lattice.

Consequently, the summation over n contains only one term when $g\neq 0$, and we find that

$$f_{\vec{g}}(s)=\begin{cases}0, & s<g\\ \dfrac{2\pi a_{\vec{g}}(0)d}{s(s^2-g^2)^{1/2}}\exp[-\frac{1}{2}(s^2-g^2)D^2] & \\ \qquad\times\cos[z_{\text{eq}}(s^2-g^2)^{1/2}], & s>g.\end{cases} \tag{3.29}$$

Although this expression is valid only when $R=\infty$, a numerical integration of Eq. (3.12) for a single plane of carbon atoms located at a distance z_{eq} from the xenon atom is straightforward. The results of such a calculation are shown in Fig. 6 for the smallest nonzero $\vec{g}$ of a graphite basal plane. It is evident that the assumption of finite R has two consequences: a small periodic component appears in $f_g(s)$ at $s<g$, and the infinite value at $s=g$ is eliminated. Of course, it should be remembered that these graphite crystallites have a distribution of radii (*and* thickness) which is of unknown width, and the literature values of radius R and thickness Z are only averages. A distribu-

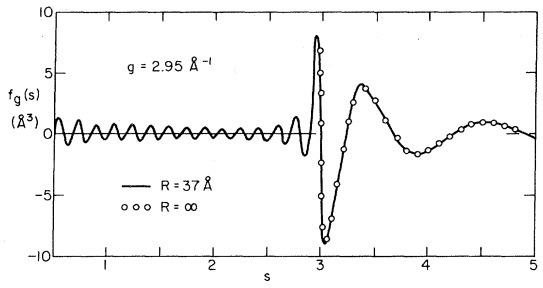

FIG. 6. Contribution to the Xe-C structure factor due to periodicity in the surface density of xenon atoms. Function $f_g(s)$ is defined by Eqs. (3.12) and (3.13). Calculations were carried out assuming vibration perpendicular to the surface with a rms amplitude of $D = 0.25$ Å. Points were calculated for a single plane of carbon atoms of infinite size using Eq. (3.29) with $a_g(0) = 1$, and the solid curve is the result of a numerical integration of Eq. (3.12) with the upper limit of τ set equal to 37 Å, but with all other parameters of the calculation taken to be identical to those for the infinite plane.

tion of R would tend to give a distribution of periodicity in Fig. 6 at $s < g$ which should average out to be quite small (except as $s \to 0$). Our conclusion is thus that the $f_g(s)$ for $R = \infty$ are a reasonable approximation to the true value except at the point $s = g$, where a peak of finite height is anticipated for real crystallites. Note also that the next set of g vectors with lengths longer than 2.95 Å^{-1} occurs at 5.11 Å^{-1} for the graphite basal plane; since the reliable part of our experimental data comes mainly at $s < 5$ Å^{-1}, the only periodic terms in $\rho_{\text{Xe-C}}(\vec{r})$ which could affect the data are those that give rise to the curve in Fig. 6.

We now consider the nonperiodic contribution to the Xe-C scattering. Equation (3.15) can be summed over planes with the aid of Eqs. (3.19) [or the more refined Eq. (3.26)] and (3.21); we find

$$f_0(s) = \left(\frac{2\pi d}{s^2}\right) \exp(-\tfrac{1}{2} s^2 D^2) \sum_{n=0}^{N_z-1} \cos[s(z_{\text{eq}} + nd)] - \cos\{s[R^2 + (z_{\text{eq}} + nd)^2]^{1/2}\}. \quad (3.30)$$

After averaging over a distribution of R values, the last term in the sum in Eq. (3.30) should become quite small (except at very small s); we therefore neglect it. The first summation in Eq. (3.30) can be done in closed form to give

$$f_0(s) = \frac{2\pi d}{s^2} \exp(-\tfrac{1}{2} s^2 D^2) \frac{\sin\frac{1}{2} N_z ds}{\sin\frac{1}{2} ds} \times \cos\{[z_{\text{eq}} + \tfrac{1}{2}(N_z - 1)d]s\}. \quad (3.31)$$

We use some elementary trigonometric identities to rewrite Eq. (3.31) in a way that shows the periodicity of $f_0(s)$ more clearly:

$$f_0(s) = \frac{\pi d}{s^2} \exp(-\tfrac{1}{2} s^2 D^2) \{\cos(sz_{\text{eq}})[\sin(sN_z d) \cot(\tfrac{1}{2} sd) + 1 - \cos(sN_z d)] + \sin(sz_{\text{eq}})\{\sin(sN_z d) - [1 - \cos(sN_z d)] \cot(\tfrac{1}{2} sd)\}\}. \quad (3.32)$$

Whenever $s = 2\pi j/d$ (where j is an integer), $f_0(s)$ will have a sharp maximum or minimum given by

$$f_0(s_{\max}) = (-1)^j \left(\frac{N_z d^3}{2\pi j^2}\right) \cos\left(\frac{2\pi j z_{\text{eq}}}{d}\right). \quad (3.33)$$

A determination of these peak heights for several values of j would appear to give an excellent method for determining z_{eq}. Unfortunately, these peaks overlap the (00l) peaks from the bare surface which occur at $s = \pi l/d_0$, where d_0 is the interplanar spacing when no adsorbate is present. Thus, precise measurements of the Xe-C peak heights is greatly complicated by the presence of large background scattering.

Of course, this calculation is not yet complete because we have not averaged over the distribution of thicknesses that exists in a real powdered sample of graphon. If this distribution is reasonably broad, the effect of such averaging upon Eq. (3.32) will be to reduce the size of the periodic terms with arguments $sN_z d$ except in the vicinity of $s = 2\pi j/d$, where peaks will still appear with heights given by Eq. (3.33). (Recollect that N_z is actually the average number of planes in a crystallite.)

As an illustration of the anticipated behavior of $f_0(s)$, several curves are shown in Fig. 7 for $z_{\text{eq}} = 3.6$ Å and different distributions of crystallite thickness, as characterized by the root-mean-square spread (δN_z) about the mean (N_z). The first two peaks in the function are shown, and the width and position of the (002) substrate peak is also indicated. It is evident that most of the intensity in $f_0(s)$ comes either at small s or in the peaks which overlap the substrate scattering. Figure 8 shows $f_0(s)$ for two values of z_{eq} with a reasonably broad distribution of δN_z; it can be seen that this function is not particularly sensitive to z_{eq}.

We now consider the Xe-Xe contribution to the diffracted intensity. Assuming first that the adatoms form a strictly two-dimensional layer, we have

$$\rho_{\text{Xe-Xe}}(\vec{r}) = \delta(z)\, \rho^{(2D)}_{\text{Xe-Xe}}(\vec{\tau}). \quad (3.34)$$

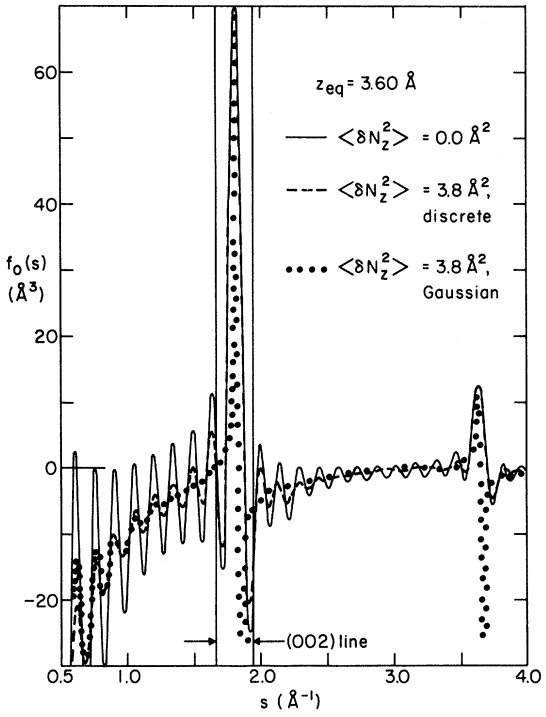

FIG. 7. Contribution to the Xe-C structure factor due to the nonperiodic part of the xenon surface density. All curves were calculated using a equilibrium gas-solid distance z_{eq} = 3.60 Å; the solid curve was obtained from Eq. (3.31) using N_Z = 12, D = 0.25 Å, and d = 3.44 Å; the dotted curve for Gaussian distribution of N_Z having breadths indicated by the mean square $\langle \delta N_Z^2 \rangle$, and the dashed curve is for a discrete distribution of δN_Z that approximates a Gaussian and has the same mean-square spread as the continuous distribution.

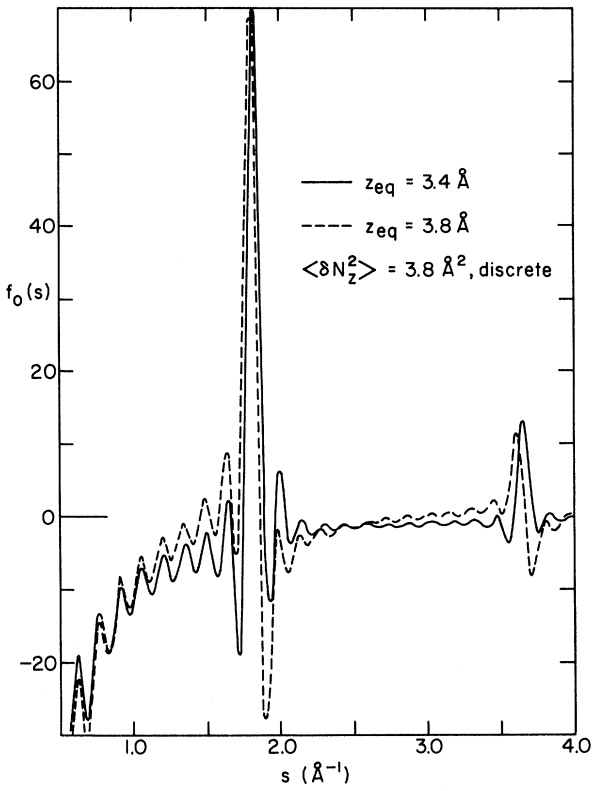

FIG. 8. Nonperiodic contribution to the Xe-C scattering is shown here for two values of the surface separation. Both curves were calculated for the discrete distribution of crystallite thicknesses used in Fig. 7; explicitly, this is: 40%, N_Z = 12; 12.5%, N_Z = 11, 13; 7.5%, N_Z = 10, 14; 5%, N_Z = 9, 15; 3%, N_Z = 8, 16; 1.5%, N_Z = 7, 17; 0.5%, N_Z = 6, 18.

After substituting $\rho_C = 0.110$ molecules/Å^3, we have

$$\tfrac{1}{2} H_{\text{Xe-Xe}}(s) = 4.55 \int \frac{\sin s\tau}{s\tau} \rho^{(2D)}_{\text{Xe-Xe}}(\vec{\tau})\, d\vec{\tau} \qquad (3.35)$$

(in units of Å^3). As a more accurate assumption would allow for small vibrational amplitudes of the xenon atoms which would give rise to a Debye-Waller factor which is evaluated in the Appendix, and gives

$$\tfrac{1}{2} H_{\text{Xe-Xe}}(s) = 4.55\, e^{-s^2D^2/3} \int \frac{\sin s\tau}{s\tau} \rho^{(2D)}_{\text{Xe-Xe}}(\vec{\tau})\, d\vec{\tau}. \qquad (3.36)$$

Although general expressions for $\rho^{(2D)}(\vec{\tau})$, the density of xenon adatoms in a monolayer at a point $\vec{\tau}$ when an adatom is known to be at the origin, are not known, this function can be calculated for the two limiting cases treated previously.

(a) For a completely mobile classical film, one writes

$$\rho^{(2D)}_{\text{Xe-Xe}}(\tau) = \Gamma G_{2D}(\tau)\,, \qquad (3.37)$$

where Γ is the surface density in molecules/Å^2 and is related to the fractional surface coverage θ in the xenon layer by

$$\Gamma = 6.0 \times 10^{-2}\theta\,. \qquad (3.38)$$

Computer simulations[22] as well as theoretical calculations[23] of $G_{2D}(\tau)$, the two-dimensional pair correlation of a classical gas on a completely flat surface, have been reported. These results can be used to evaluate

$$h(s) = \frac{2\pi}{s} \int_0^\infty \sin(s\tau)[G_{2D}(\tau^*) - 1]\, d\tau^*\,, \qquad (3.39)$$

where τ^* is the reduced distance τ/σ. The final expression for $H_{\text{Xe-Xe}}(s)$ now becomes

$$\tfrac{1}{2} H_{\text{Xe-Xe}}(s) = 0.27\sigma_{\text{Xe}}\, \theta h(s) e^{-s^2D^2/3}\,, \qquad (3.40)$$

where σ_{Xe}, the size parameter in the Lennard-Jones potential function for xenon atoms, is taken to be 4.0 Å. The pair correlation functions and thus $h(s)$ depend upon temperature as well as sur-

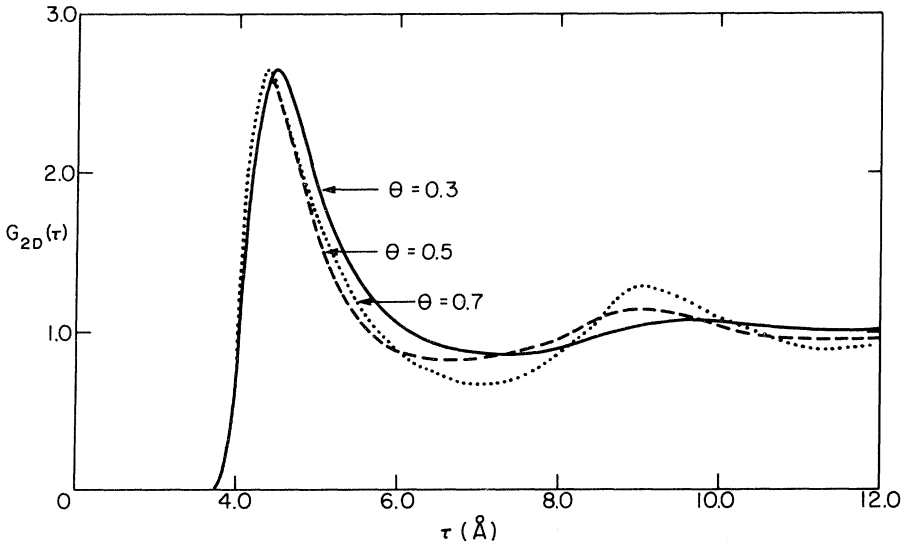

FIG. 9. Two-dimensional pair correlation functions are shown for xenon atoms on a perfectly flat surface interacting via Lennard-Jones (12-6) functions at $kT/\epsilon = 0.8$. Method of calculating these functions is described in Ref. 23.

face density. Assuming that the experimental conditions correspond to a reduced temperature $T^* = 0.8$, the correlation functions and transforms were evaluated at several surface densities. The correlation functions used are shown in Fig. 9 and the structure factors that result are plotted in Fig. 10.

(b) If the adsorbed layer forms as a dense, completely registered island on the surface,

$$\rho^{(2D)}_{\text{Xe-Xe}}(\vec{\tau}) = \sum \delta(\vec{\tau} - \vec{\tau}_R)\,, \tag{3.41}$$

where $\vec{\tau}_R$ denotes a xenon-xenon separation vector in the registered film. The structure factor for this model is

$$\tfrac{1}{2} H_{\text{Xe-Xe}}(s) = 4.55 e^{-s^2 D^2} \sum_t n_t \frac{\sin s\tau_t}{s\tau_t}\,, \tag{3.42}$$

where n_t is the number of atoms at distance τ_t. In particular, the distances τ_t for a $\sqrt{3} \times \sqrt{3}$ registered phase on the graphite basal plane are given by

$$\tau(m,n) = a[(m + \tfrac{1}{2}n)^2 + \tfrac{3}{4}n^2]^{1/2} \tag{3.43}$$

with m and n equal to integers which would range from $+\infty$ to $-\infty$ for a registered film of infinite area. Figure 11 shows the structure factors that result when two finite values of the radius of the crystallite are assumed. For radii as large as 25 Å, the Bragg peaks, which occur at $s = 1.70$, 2.95, 3.41,... (Å^{-1}) for the $\sqrt{3} \times \sqrt{3}$ lattice, are visible, together with ripple resulting from the truncation. As the radius of the registered region R_{Xe} is increased, the heights of the Bragg peaks increase as expected. A distribution of R_{Xe} values should smear out all the ripple, leaving only the Bragg peaks. Unfortunately, the first Bragg peak in this model tends to overlap first Xe-C peak as well as the (002) substrate scattering, giving rise to resolution problems for adsorbed layers occurring as registered lattices on this surface.

If we now contrast the structure factors $H_{\text{Xe-Xe}}(s)$ for the completely mobile film and for the registered film, we see that a peak occurs at $s \simeq 1.7$ Å^{-1} in both cases; the peak is sharper and is followed by additional peaks in the registered

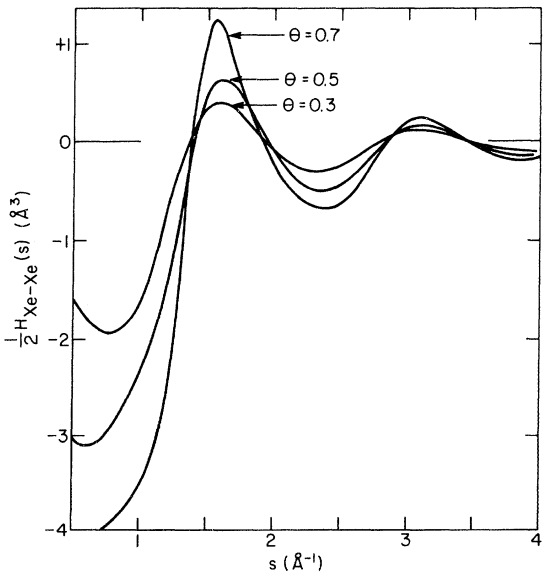

FIG. 10. Fourier transforms of the pair correlation functions of Fig. 9 are shown here. The structure factor $H_{\text{Xe-Xe}}(s)$ is defined by Eqs. (3.39) and (3.40); the rms vibrational amplitude D was taken to be 0.25 Å and values of the fractional surface coverage θ are indicated in the figure.

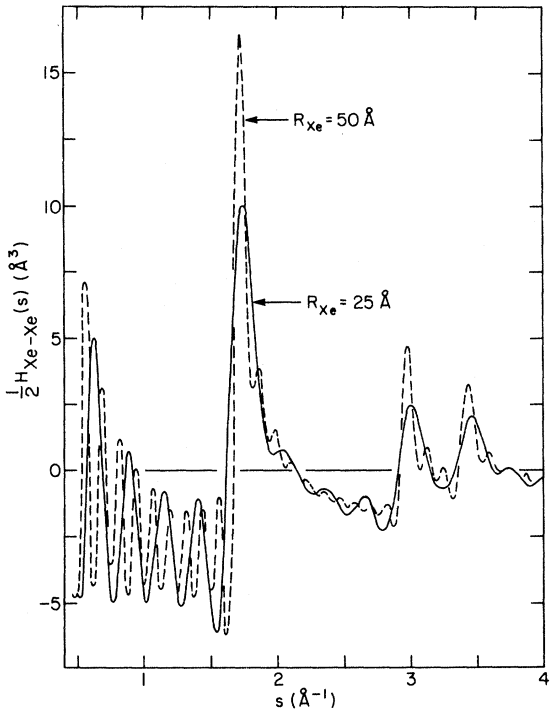

FIG. 11. Structure factors for a $\sqrt{3} \times \sqrt{3}$ registered xenon monolayer of finite radius R. Equation (3.42) was evaluated by direct summation for $\tau_R < R$ using $D = 0.25$ Å.

film. If one assumes that the size of the registered regions increases with increasing coverage, one concludes that the peak heights for both models will increase with increasing coverage. The near coincidence of the locations of the first peaks in the structure functions for the two models reflects the fact that the short-range order which causes the peak in the mobile film case is associated with a most probable separation distance of 4.4 Å (as shown by the pair correlation functions of Fig. 9), and it happens that this is quite close to the nearest-neighbor separation of 4.26 Å in the registered lattice.

We close this section by noting that the radial distribution function shown in Fig. 4 can now be expressed in terms of the theory presented here. If we write $z = r\cos\theta$ and $\tau_{ij}^2 = z_{ij}^2 + r_{ij}^2$, we see that an average of $g(\vec{\tau}, z)$ over all values of $\cos\theta$ is needed to obtain the desired function of r. In order to do this explicitly here, we make the simple assumption that the amplitude of vibration perpendicular to the surface is negligible. In this case, $\tau_{ij}^2 = r_{ij}^2$ and

$$\rho_{Xe-Xe}^{(2D)}(\tau) = \rho_{Xe-Xe}^{(2D)}(r) . \tag{3.44}$$

Furthermore,

$$G_{\vec{g}}(r\cos\theta) = \frac{d}{r} \sum_{n=0}^{N_g - 1} a_{\vec{g}}(n)\, \delta(\cos\theta - (z_{eq} + nd)/r) . \tag{3.45}$$

If we consider only the term with $\vec{g} = 0$, Eq. (3.11) can be averaged over $\cos\theta$ to give

$$G_{Xe-C}(r) = \frac{d}{2r} \sum_{n=0}^{\infty} H(r - (z_{eq} + nd)) ;$$

$$G_{Xe-C}(r) = \begin{cases} 0, & r < z_{eq} ; \\ \dfrac{d}{2r}, & z_{eq} < r < z_{eq} + d ; \end{cases} \tag{3.46}$$

where $H(x)$ is the Heaviside step function. Thus, the experimental $\rho(r)$ would be expected to exhibit coverage dependent peaks due to the Xe-Xe correlations plus a series of jumps occuring at $r = z_{eq}$; $z_{eq} + d$; etc. Presumably the effect of vibrational motion perpendicular to the surface would be to smear out all of these features, thus giving rise to theoretical curves that are similar to those shown in Fig. 4. Rather than carrying this approach further, we will attempt to compare experimental and theoretical structure factors in Sec. IV.

IV. DISCUSSION

Experimental structure factors for adsorbed xenon at three surface coverages are shown in Fig. 3, and the uncertainties introduced in the construction of these curves from the raw data have already been discussed in Sec. II. The plot of $\Phi(s) = [f_{Xe}(s)/f_{Xe}(0)]^2$ which is shown in Fig. 5 shows quite clearly that a small error in the estimation of the single-particle scattering at s between 5 and 6 Å^{-1} can give rise to rather large uncertainties in the scattering factors when s is between 1 and 3 Å^{-1}.

With this in mind, we can understand some of the features of the experimental $H(s)$ curves in Fig. 3. In the first place, the peaks that might lead one to deduce the presence of a registered xenon layer are absent; at least three such peaks should be observable in the experimental range (at values of s indicated in Fig. 11). In fact, the data support the belief that a registered ordered monolayer for this system is quite unlikely at a temperature as high as that used in this work. It also indicates that there are no abrupt changes in atomic ordering over the coverage range of the experiments and thus rules out the occurrence of phase changes in these adsorbed films.

It is anticipated that the Xe-C part of scattering will be essentially independent of coverage. If the Xe-Xe part is due to a mobile film possessing only short-range order, the analysis given in

Sec. III indicates that the Xe-C scattering should be dominant when the coverage is as small as 0.24. If this is indeed the case, one expects to observe a sharp peak at $s \simeq 1.8$ Å^{-1} and a less-pronounced one at $s \simeq 3.6$ Å^{-1}. Both features are present for $\theta = 0.24$, although the first peak is displaced to $s = 1.65$ Å^{-1} and the second peak appears to be considerably broader than theory would predict. A shift in the position of the first peak has also been observed in neutron scattering from argon adsorbed on this solid,[24] and its displacement is probably due to a change in the layer spacing of the solid upon absorption (i.e., swelling of the adsorbent). The increased breath of the second peak could be taken as an indication that the true Debye-Waller factors involve a D value larger than that assumed here.

The curves for the two high coverages again show two peaks; however, they are shifted in toward smaller s (relative to those for the low coverage structure factor) and have also increased in intensity. If we assume that the Xe-Xe correlations contribute to the scattering at high θ but not at low, both effects may be explained. For example, the first peak shown in Fig. 10 for the Xe-Xe structure factor at high coverage occurs at $s \simeq 1.5$ Å. With increasing coverage, we might anticipate that the first peak becomes a composite of Xe-C and Xe-Xe mobile film peaks, with a position that gradually moves inward as θ increases. Note also that the theoretical mobile film structure factors shown in Fig. 10 exhibit broad maxima at s between 2.9 and 3.5 Å^{-1}. This feature also appears in the experimental curves, but is displaced slightly toward smaller s (as is also true for the second peak in the low coverage curve).

To summarize, the positions of the peaks in the experimental structure factors and the variation in position with increasing coverage seem to be consistent with a picture in which the excess scattering at low coverage is due to Xe-C correlations; that no contributions due to possible periodic components in the xenon surface density are observed at any coverage, and that the high coverage results are due to a superposition of Xe-C and Xe-Xe mobile film scattering.

As yet unexplained is the rather large background scattering in $H(s)$ at high coverage. This manifests itself by the large height of the second peak relative to the first and by the fact that this second peak is also broader than expected. No reasonable assessment of experimental and computational uncertainties would remove the difference between these results and the theoretical predictions. Thus we should seek a real physical reason for the discrepancy. A possible source arises from the fact that the calculations are based on the assumption that the adsorbed atoms are on a single, perfectly flat surface, the total effect thus being the sum of the scattering from individual crystallites. This ignores scattering from the xenon at other locations. Atoms are adsorbed on the sides and backs of each crystallite; at points of irregularity in the exposed basal plane; on neighboring crystallites, and in second and higher layers on the surface. (Even when the nominal θ is less than one, computer simulations[25] and theoretical arguments[26] indicate that not all atoms go into the monolayer. Instead, filling in the second layer begins before the first layer is complete. Of course, when the nominal θ is greater than unity, the number of atoms in higher layers increases quite rapidly.) However, our knowledge of the number and exact position of such atoms is still too limited to allow a precise estimate of their effect upon the scattering. In general, we hypothesize that such effects would give rise to a range of distances, each characterized by a $(\sin sr)/sr$ term in the structure factor, and that the summation of these peaks might well give rise to an apparent increase in the background scattering. We emphasize that a 10% shift in the estimated value of f^2 would bring $H(s) = \Delta I(s)/f_{\mathrm{Xe}}^2 - 1$ to within 10% of the expected behavior and would shift the peak positions by no more than 0.2 Å^{-1}. Thus, these difficulties in explaining the appearance of excess background scattering should not be allowed to obscure the fact that the agreement between experiment and theory is quite satisfactory in most respects.

We can conclude that these experiments show that quantitative measurements of x-ray scattering by selected atoms adsorbed on well-characterized surfaces are feasible, even at coverages less than monolayer, and that the resulting data contain considerable useful information about the correlations between adatom positions relative to the solid lattice and to each other. Clearly, studies of this and other systems over a range of temperature would be of interest; it is hoped that the work reported here will help stimulate such investigations.

APPENDIX

Derivations of the Debye-Waller expression for the temperature dependence of peak heights in x-ray or neutron scattering from a crystal are based on the assumption that s^2D^2 is small compared to unity. When these ideas are applied to a calculation of the effect of vibration perpendicular to the surface upon the scattering from a physisorbed monolayer film, one finds that this assumption is not necessarily an accurate one. Specifically, if the estimated root-mean-square amplitude D is

0.25 Å for xenon on graphitized carbon, the product sD will be of the order of unity over much of the experimental range of s. This necessitates a careful calculation of the effects of this motion upon the scattering.

We start from the premise that the motion upon the scattering perpendicular to the surface is harmonic, classical, and uncorrelated to the perpendicular motions of neighboring adatoms. In this case, the distribution of gas-solid distances is given by Eq. (3.26), with a mean-square amplitude $D^2 = kT/k_z$, with k_z equal to the curvature of the gas-solid energy curve at its minimum. The problem arises in the calculation of $H_{\text{Xe-Xe}}(s)$, the Xe-Xe structure factor which involves z_{ij}, $\tau_{ij} = r_{ij}$, the relative distance between xenon atoms i and j. The analog of Eq. (3.26) for the distribution of z_{ij} is

$$W(z_{ij}) = (1/2D\sqrt{\pi})\, e^{-z_{ij}^2/4D^2}. \tag{A1}$$

The aim here is to derive an expression that will replace the structure factor given in Eq. (3.36) by a more accurate result; this means that we wish to evaluate

$$I(\tau_{ij}) = \int_{-\infty}^{\infty} \frac{\sin(sr_{ij})}{sr_{ij}}\, W(z_{ij})\, dz_{ij}. \tag{A2}$$

We write

$$\frac{\sin sr_{ij}}{sr_{ij}} = \left(\frac{\pi}{2}\right)^{1/2} \frac{J_{1/2}\left(s(\tau_{ij}^2 + z_{ij}^2)^{1/2}\right)}{\left[s(\tau_{ij}^2 + z_{ij}^2)^{1/2}\right]^{1/2}} \tag{A3}$$

and use the addition theorem for Bessel functions to show

$$\frac{\sin sr_{ij}}{sr_{ij}} = \frac{\sqrt{\pi}}{2} \sum_{m=0}^{\infty} (-1)^m \frac{(4m+1)\Gamma(m+\frac{1}{2})}{m!} \times \frac{J_{2m+1/2}(s\tau_{ij})\, J_{2m+1/2}(sz_{ij})}{(s\tau_{ij})^{1/2}(sz_{ij})^{1/2}}. \tag{A4}$$

At this point, the integration over z_{ij} can be performed with the aid of

$$\int_0^{\infty} \frac{J_{2m+1/2}(sz)}{(sz)^{1/2}}\, e^{-z^2/4D^2}\, dz = \frac{D\Gamma(m+\frac{1}{2})}{\sqrt{2}\,\Gamma(2m+\frac{3}{2})} \times (sD)^{2m}\, {}_1F_1(m+\tfrac{1}{2}, 2m+\tfrac{3}{2}, -s^2D^2), \tag{A5}$$

where ${}_1F_1(a,c,x)$ is the confluent hypergeometric function. When Eqs. (A4) and (A5) are substituted into Eq. (A2), the result can be written

$$I(\tau_{ij}) = \sum_{m=0}^{\infty} I_m j_{2m}(s\tau_{ij}) \tag{A6}$$

with

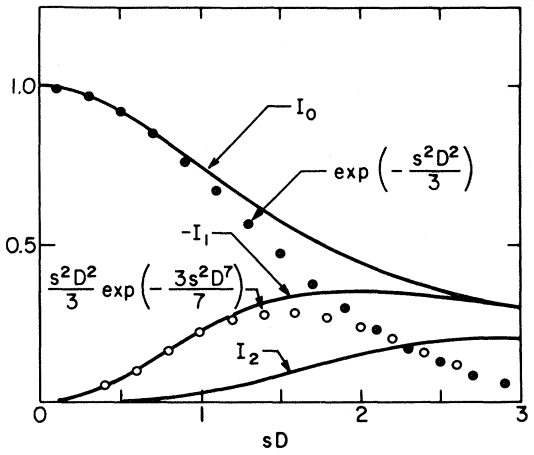

FIG. 12. Functions I_m defined by Eq. (A7) are plotted vs the dimensionless parameter sD. Points show approximations to these functions which should be most accurate at small values of sD.

$$I_m = (-s^2D^2)^m \frac{(4m+1)[\Gamma(m+\frac{1}{2})]^2}{2m!\,\pi\Gamma(2m+\frac{3}{2})} \times {}_1F_1(m+\tfrac{1}{2}, 2m+\tfrac{3}{2}, -s^2D^2). \tag{A7}$$

Up to this point, no approximations concerning the magnitude of sD have been introduced; we can compare the results of Eqs. (A6) and (A7) with Eq. (3.36) by writing out the first few terms in the series expansions for the confluent hypergeometric functions. We find that

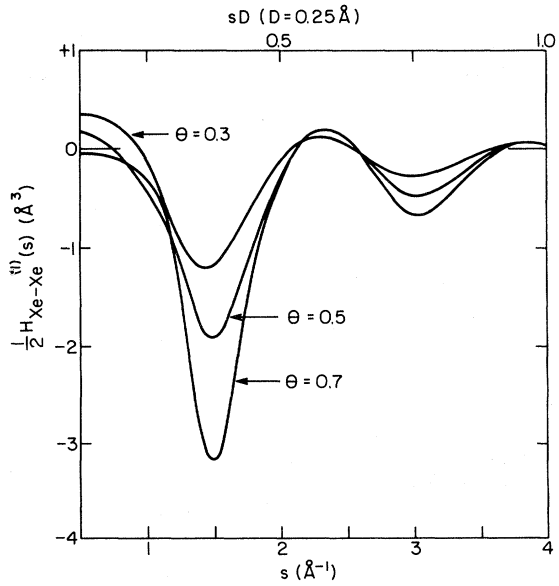

FIG. 13. Spherical Bessel transform of the pair correlation functions for mobile xenon film is shown here for the Bessel function $j_2(s\tau)$, giving the partial structure factor $H^{(1)}_{\text{Xe-Xe}}(s)$ defined in Eq. (A13).

$$I_0 = (1 - \tfrac{1}{3}s^2D^2 + \tfrac{1}{10}s^4D^4 + \cdots),$$
$$I_1 = -\tfrac{1}{3}s^2D^2(1 - \tfrac{3}{7}s^2D^2 + \cdots), \quad \text{(A8)}$$
$$I_2 = \tfrac{3}{70}s^4D^4(1 + \cdots).$$

If one takes the limit of these functions as $s^2D^2 \to 0$, Eq. (A6) reduces to

$$I(\tau_{ij}) = (\sin s\tau_{ij})/s\tau_{ij}. \quad \text{(A9)}$$

However, this procedure gives no "Debye-Waller" factor. Thus we retain terms of order s^4D^4 in Eq. (A8) to arrive at approximate I_m which are

$$I_0 = e^{-s^2D^2/3}(1 + \tfrac{2}{45}s^4D^4 + \cdots), \quad \text{(A10)}$$
$$I_1 = -\tfrac{1}{3}s^2D^2e^{-3s^2D^2/7}(1 + \cdots). \quad \text{(A11)}$$

It is clear that this procedure will give rise to a "Debye-Waller" factor but will also introduce extra contributions to the structure factor.

A general expression for the structure factor that does not involve power series in s^2D^2 can be written

$$H_{\text{Xe-Xe}}(s) = \sum_{m=0}^{\infty} I_m H^{(m)}_{\text{Xe-Xe}}(s) \quad \text{(A12)}$$

with

$$\tfrac{1}{2}H^{(m)}_{\text{Xe-Xe}}(s) = 4.55 \int j_{2m}(s\tau)\, \rho^{(2D)}_{\text{Xe-Xe}}(\tau)\, d\tau. \quad \text{(A13)}$$

Some plots of I_m as a function of sD are shown in Fig. 12. The spherical Bessel-function transform that gives $H^{(m)}_{\text{Xe-Xe}}(s)$ for $m = 1$ was calculated using the $G_{2D}(\tau)$ shown in Fig. 9. The results are plotted in Fig. 13. The curves in Fig. 12 indicate that the simple equations for I_0 and I_1 are reasonably accurate up to $sD \simeq 1$; since this corresponds to $s \simeq 4$ Å^{-1} for our estimate of D, we have used Eqs. (A10) (without the term in s^4D^4) and (A11) to calculate the Xe-Xe structure factor for a mobile film with $\theta = 0.7$. When the component contributions to $\frac{1}{2}H_{\text{Xe-Xe}}(s)$ are evaluated, it is found that the term with $m = 1$ makes only a small contribution to the total when $D = 0.25$ Å. When it is included, its main effect is to slightly increase the height of the peaks in the $m = 0$ function.

Of course, a calculation of the structure factor for a registered xenon film should also include contributions for $m = 1$, etc.; these terms have not been evaluated because (a) Debye-Waller factors for vibrations parallel to the surface in the registered layer should also be included, and (b) the scattering factor for this model is dominated by sharp peaks which means that detailed intensity variations are not as important as in the case of the mobile film. We have attempted to take the three-dimensional vibrations into account crudely in Eq. (3.42) by using a Debye-Waller factor of $e^{-s^2D^2}$ rather than $e^{-s^2D^2/3}$.

*Present address: Division of Laboratories and Research, N.Y. State Dept. of Health, New Scotland Avenue, Albany, N.Y. 12201.

[1]W. A. Steele, *The Interaction of Gases with Solid Surfaces* (Pergamon, Oxford, 1974).
[2]J. G. Dash, *Films on Solid Surfaces* (Academic, New York, 1975).
[3]A. Thomy and X. Duval, J. Chem. Phys. 67, 1101 (1970); X. Duval and A. Thomy, Carbon 13, 242 (1975).
[4]F. A. Putnam and T. Fort, J. Phys. Chem. 79, 459 (1975).
[5]G. D. Huff and J. G. Dash, Phys. Rev. A (to be published).
[6]A. A. Antoniou, P. H. Scaife, and J. M. Peacock, J. Chem. Phys. 54, 5403 (1971).
[7]M. Bretz and T. T. Chung, J. Low Temp. Phys. 17, 479 (1974).
[8]J. J. Lander and J. Morrison, Surf. Sci. 6, 1 (1967); H. M. Kramer and J. A. Venables, J. Cryst. Growth 17, 329 (1972); J. Suzanne, J. P. Coulomb, and M. Bienfait, Surf. Sci. 40, 414 (1973); J. P. Coulomb, J. Suzanne, M. Bienfait, and P. Masri, Solid State Commun. 15, 1585 (1974).
[9]J. K. Kjems, L. Passell, H. Taub, and J. G. Dash, Phys. Rev. Lett. 32, 724 (1974); J. K. Kjems, L. Passell, H. Taub, J. G. Dash, and A. D. Novaco, Phys. Rev. B 13, 1446 (1976); H. Taub, L. Passell, J. K. Kjems, K. Carniero, J. P. McTague, and J. G. Dash, Phys. Rev. Lett. 34, 654 (1975).
[10]George W. Brady and Martin L. Kaplan, J. Chem. Phys. 58, 3535 (1973).
[11]G. W. Brady, C. Cohen-Addad, and E. F. X. Lyden, J. Chem. Phys. 51, 4309 (1969); N. S. Gingrich, Rev. Mod. Phys. 15, 90 (1943).
[12]H. Cochrane, P. L. Walker, Jr., W. S. Diethorn, and H. C. Friedman, J. Colloid and Interface Sci. 24, 405 (1967).
[13]B. E. Warren, *X-Ray Diffraction Procedures* (Addison-Wesley, Reading, Mass., 1969), pp. 116–119.
[14]J. Waser and V. Schomaker, Rev. Mod. Phys. 25, 671 (1953). This paper gives a detailed discussion of termination and other errors encountered in Fourier transform techniques.
[15]A. H. Narten, M. D. Danford, and A. A. Levy, ORNL report 3997 (1966) (unpublished); Disc. Faraday Soc. 43, 97 (1967).
[16]N. N. Avgul and A. V. Kiselev, in *Chemistry and Physics of Carbon*, edited by P. L. Walker, Jr. (Dekker, New York, 1970), Vol. 6.
[17]C. R. Houska and B. E. Warren, J. Appl. Phys. 25, 1503 (1954).
[18]B. E. Warren, in *Proceedings of the Second Conference on Carbon* (University of Buffalo, Buffalo, 1956), p. 49.
[19]W. A. Steele, Surf. Sci. 36, 317 (1973); A. D. Crowell and D. M. Young, Trans. Faraday Soc. 49, 1080 (1953); N. N. Avgul, A. V. Kiselev, I. A. Lygina, and D. P.

Poshkus, Bull. Acad. Sci. USSR Div. Chem. Sci. 1155 (1959).
[20]J. A. Ibers, in *International Tables for X-Ray Crystallography* (Kynoch, Birmingham, England, 1962), Vol. 3.
[21]G. N. Watson, *A Treatise on the Theory of Bessel Functions* (Cambridge U.P., Cambridge, 1962).
[22]P. F. Fehder, J. Chem. Phys. 50, 2617 (1969); 52, 791 (1970); S. Toxvaerd, Mol. Phys. 29, 373 (1975); F. Tsien and J. P. Valleau, *ibid.* 27, 177 (1974).
[23]W. A. Steele, J. Chem. Phys. (to be published).
[24]J. P. McTague (private communication).
[25]J. E. Lane and T. H. Spurling, in *Proceedings of the Fourth International Conference on Chemical Thermodynamics, Montpellier, 1975*, Aust. J. Chem. (to be published).
[26]Reference 1, p. 232.